# Direct measurement of ion evaporation kinetics from electrified liquid surfaces

M. Gamero-Castaño and J. Fernández de la Mora
*Yale University, Department of Mechanical Engineering, New Haven, Connecticut 06520-8286*

(Received 6 April 1999; accepted 10 April 2000)

When concentrated solutions of NaI in formamide with electrical conductivities $K$ larger than 1.1 S/m are electrosprayed from a Taylor cone-jet in a vacuum, ions are evaporated at substantial rates from the surface of the meniscus and the drops. This constitutes a new source of ions and nanoparticles, where the relative importance of these two contributions is adjustable. The currents of ions are measured independently from those associated with drops by a combination of stopping voltage analysis and preferential scattering in a gas background. The magnitude $E$ of the electric field at the surface of the drops and at the apex of the cone-jet is controlled through the electrical conductivity $K$ of the liquid and its flow rate $Q$ through the jet. $E$ is related through available scaling laws for Taylor cone-jets to the ratios $K/Q$ or $I/Q$, where $I$ is the current of drops emitted by the jet. Ion currents are very small or null at typical $K/Q$ values used in the past. A relatively small initial ion current is attributed to a few particularly sharp features present, perhaps associated with small satellite drops. At still higher $K/Q$ this first ionization source saturates, and ion evaporation from the main drops begins to dominate ($E \sim 1$ V/nm). $E$ can then be determined with little ambiguity, and the associated ion current is also measured over a broad enough range of electric fields to determine the ionization kinetics. At still higher $K/Q$ the ion current from the drops approaches saturation, and ion evaporation directly from the meniscus becomes dominant. The total spray current then presents the anomaly of increasing rapidly at decreasing liquid flow rate. The ion current from the meniscus can also be measured in this regime over a broad range of $K/Q$, with qualitative agreement with the ionization measurements from the drops. But the relation established between $K/Q$ and $E$ becomes suspect because ion and drop currents are now comparable. A third approach to infer the ionization rate is based on the related disappearance of Coulomb explosions of the drops above a critical $K/Q$. These results are congruent with the model of Iribarne and Thomson, with an activation barrier for ion evaporation equal to $1.7\,\mathrm{eV} - (e^3E/4\pi\epsilon_0)^{1/2}$. © *2000 American Institute of Physics.* [S0021-9606(00)70126-7]

## I. INTRODUCTION

The phenomenon of ion evaporation from charged liquid surfaces is of considerable interest in many areas of science and technology. It is most widely exploited to produce gas phase ions from the enormous variety of those forming naturally[1] (or electrochemically[2]) in organic solvents.[3] As in conducting solids,[4] ion evaporation from liquids is activated by surface electric fields in excess of 1 V/nm.[5–7] But a liquid surface is not easily forced into a prescribed shape, a difficulty compounded by its natural instability in the presence of high electric fields.[8,9] Hence, while a great variety of ions have been seen to form from the surface of charged organic liquids, no study has succeeded yet at characterizing the shape and electric field $E$ present in the liquid surface, together with the associated ion evaporation current $I_i$. To do so is our goal here.

While earlier studies have successfully determined the electric field $E$ on a liquid surface and inferred the associated ion current $I_i$ indirectly, our present aim is to measure $I_i$ and $E$ directly. Both tasks are relatively involved. The means to fix $E$ are described in Sec. II. It is based on the fact that the curvature and surface charge density on the meniscus and the drops created by Taylor cone-jets (Fig. 1) are known approximately, and may be finely controlled through the electrical conductivity $K$ of the liquid and its flow rate $Q$ through the jet [Fig. 1(b)]. Not many electrolytes are available with which Taylor cones supporting electric fields in the range of 1 V/nm can be created in a vacuum. Hence, the identification of formamide (Sec. II C) as one such substance greatly facilitates reaching our goals. The experimental system used is described in Sec. III. Measurement of the ionization current is relatively simple, because the large disparity in mass between ions and spray drops allows their ready separation by scattering of the ions in a background gas. However, distinguishing the ions generated from the drops from those originating simultaneously from the meniscus requires the detailed data analysis of Sec. IV.

Two types of indirect experimental studies on ion evaporation have been undertaken previously. In the first, the required surface field is achieved through the evaporation of a cloud of charged drops produced by atomizing a liquid sample.[5,10,11] The ion current globally released from this mist is measurable in principle. But the radii (and charges) of the drops from which ions emanate evolve too fast and are too small (<20 nm) to be monitored. Furthermore, it is not possible to determine which among the many coexisting drop

 

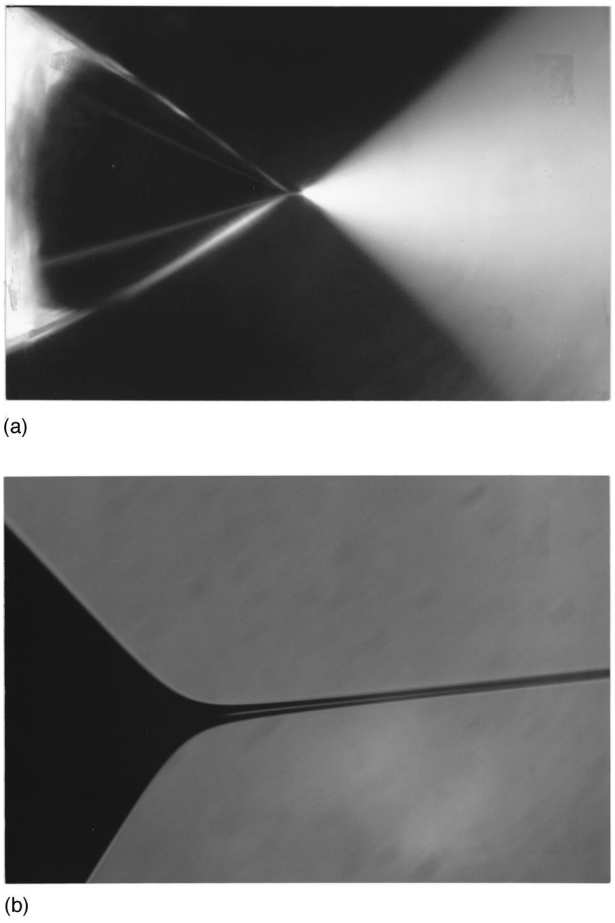

FIG. 1. Liquid meniscus and spray of charged drops in atmospheric air. (a): tributyl phosphate ($Q=10$ nl/s, $K=0.033$ S/m). (b): detail of the apex region for ethylene glycol ($Q=1.28$ $\mu$l/s, $K=2.25\times10^{-5}$ S/m).

charges and radii present in the spray are responsible for the observed ions. Nonetheless, examination of the solid residues remaining after complete drop evaporation has provided valuable information on the magnitude of these fields ($E\sim1-3$ V/nm), which has been generally interpreted as supporting the essence of the ionization model of Iribarne and Thomson.[6,7] The ionization current was inferred in Ref. 7 from some general assumptions on the high steepness of the current versus electric field curve (leading to an approximately constant electric field on the surface of ion-evaporating drops) and from the calculated solvent evaporation rate. The reduction of the activation energy for ion evaporation, $G_E(E)$, could then be measured as a function of the electric field $E$. For liquids with high dielectric constant ($\epsilon\gg1$) and drop diameters much larger than 1 nm, it was found to be in close agreement with a slightly modified form of the polarization potential model of Iribarne and Thomson:

$$G_E(E)=(e^3E/4\pi\epsilon_0)^{1/2}. \tag{1}$$

A second approach has relied on the formation of Taylor cones under vacuum. Their tip curvatures and associated fields are known to span many orders of magnitude, depending mainly on the electrical conductivity $K$ of the liquid. Hence, Taylor cones of liquid metals ($K\sim10^6$ S/m) tend to emit mostly single metal ions.[12] Taylor cones of exceptionally conducting electrolytes such as $SO_4H_2$ ($K\sim10$ S/m) appear to yield primarily solvated ions,[13] although this situation has been investigated only to a very limited degree. Concentrated salt solutions in glycerol ($K\sim10^{-2}$ S/m) emit mostly micrometer and sub-micrometer drops. But, when driven under very high voltages ($\sim15$ kV rather than $\sim3$ kV) with hundreds of individual Taylor cones on the rim of the supply capillary electrode, they do also yield measurable quantities of ions and clusters.[14,15] But not enough is known on this high-voltage regime for the magnitude of the field and the ionization surface to be predictable.

A single Taylor cone in a vacuum provides a simpler way to measure the current of field-evaporated ions, and hence investigate directly the kinetics of this phenomenon. But this approach must face the difficulty of determining the geometry and the distribution of fields on the drops and the cone tip, with radii of curvatures in the range of 10–20 nm. Several electron microscope studies have already examined the shape of liquid metals tips,[12] and observed radii of curvature in the nanometer range.[12a] However, no control of the magnitude of the surface electric field has been achieved, and is unlikely to be achieved with liquid metals.[16] The reason is that, for all known metals and all attainable experimental conditions, their electrical conductivity is large enough to make the Taylor cone effectively equipotential down to the tip,[12b,c] with curvatures large enough for ion evaporation to always be dominant.[12]

Organic liquids offer the large advantage over liquid metals that the surface electric field $E$ can be controlled in their Taylor cones through its dependence on $K$, which can itself be varied widely through the electrolyte concentration. $E$ can also be controlled through the dependence of the tip curvature on the flow rate $Q$ of liquid pushed through the cone, which in this case develops into a jet, and then breaks into drops [spray in Fig. 1(a)]. This freedom is in fact the key to the present investigation, where the measurement of the ion current $I_i$ as a function of the variables $K$ and $Q$ will be converted into the desired ionization kinetics curve $I_i(E)$.

## II. CONTROLLING THE ELECTRIC FIELD IN THE V/nm RANGE

This section addresses two key difficulties that have hindered controlling the electric field on the surface of a liquid in the range of 1 V/nm. The link between controllable variables in Taylor cone-jets and the corresponding electric fields in the meniscus and the spray drops is established in Secs. II A and II B. For readers wishing to skip the full argument, it is enough to know that the quantities $E_k$ and $E_I$ defined in Eqs. (5a) and (5b) multiplied by suitable factors of the order of 1 are the appropriate fields present on the meniscus and the drops respectively. Section II C discusses the physical properties required for a liquid to be able to access the V/nm range, and proposes formamide as a suitable solvent.

### A. The electric field in the cone-jet

Several recent experimental and theoretical investigations on the scaling laws of cone-jets have clarified the dependence of the meniscus geometry and surface charge on

liquid properties and the variables $Q$ and $K$. The electric field $E$ normal to the surface of a Taylor cone has long been known to be given by the local radius $R$ and semi-angle $\alpha$ (49.29°) of the cone, the surface tension $\gamma$ of the liquid and the electrical permittivity of vacuum $\epsilon_0$:[17]

$$E=2[\gamma\cos\alpha/(\epsilon_0 R)]^{1/2}. \tag{2}$$

This field increases as the apex is approached from the cone side, but not without limit, because the cone eventually degenerates into a jet. In the far downstream region of the jet, most of the current travels by convection, and the electric field inside the liquid is much smaller than outside. The charge density $dq/dx$ per unit axial length is hence the ratio $I/U$ between the jet current and its speed, so that Gauss' law gives the normal electric field as

$$E=RI/(2Q\epsilon_0), \tag{3}$$

which also increases as the apex is approached from the jet side. The maximum electric field normal to the surface must therefore occur somewhere in the transition region between the cone and the jet. There, Eqs. (2) and (3) become comparable, so that $R^3\sim 8\cos\alpha\gamma Q^2\epsilon_0/I^2$, and $E^3\sim\gamma I\cos\alpha/(\epsilon_0^2 Q)$. We therefore introduce the characteristic electric field and jet radius $E_I$ and $R_I$:

$$R_I\equiv(8\gamma Q^2\epsilon_0/I^2)^{1/3}; \tag{4a}$$

$$E_I\equiv[\gamma I/(\epsilon_0^2 Q)]^{1/3}. \tag{5a}$$

These quantities are based on the readily measurable spray current (subscript $I$). Approximate experimental scaling laws available for this current show that[18–20]

$$I=F(\epsilon)[\gamma KQ]^{1/2}, \tag{6}$$

where the quantity $F(\epsilon)$ has been measured for a number of liquids with dielectric constants $\epsilon$ ranging from 9 to 200, and takes in all cases values of order unity. This result is also confirmed by theory,[18,21] though not yet with the numerical analysis required at the apex region to give precise values for the function $F(\epsilon)$. Inserting Eq. (6) in the expression for $R_I$ and $E_I$, one finds characteristic values $R_K$ and $E_K$ for the radius of curvature and electric field in the region of maximum electric field:

$$R_K\equiv[\epsilon_0 Q/K]^{1/3}; \tag{4b}$$

$$E_K\equiv\frac{\gamma^{1/2}K^{1/6}}{\epsilon_0^{2/3}Q^{1/6}}, \tag{5b}$$

now based on the electrical conductivity of the liquid rather than the jet current (subscripts $K$). The value $R_K$ arrived at in Eq. (4b) is found experimentally to be closely related to the mean diameter $\langle D_d\rangle$ for the drops into which the jet breaks,[22,19,20]

$$\langle D_d\rangle=G(\epsilon)R_K, \tag{7}$$

where the proportionality constant $G(\epsilon)$ is also a quantity of order one for all values of the dielectric constant $\epsilon$ for which data are available. $R_K$ is also easily interpreted as a *charge relaxation length*, or the characteristic cone radius $R$ where the fluid dynamic time $\sim R/U\sim R^3/Q$ becomes comparable with the electrical relaxation time $\epsilon_0/K$.[23,18] Interestingly, this determination of $R_K$ is independent of the scaling law for the current. Hence, the characteristic field $E_K$ is just Taylor's field Eq. (2) when $R$ is the charge relaxation length. This, together with the fact that the current associated to surface convection at the point of maximum field is still several times smaller than the total spray current, makes $E_K$ a more natural variable than $E_I$ to describe the maximum electric field on the meniscus. Alternatively, $E_I$ is probably more appropriate to describe the characteristic field in the final jet region. We shall see in Sec. II B that $E_I$ provides also the right scale for the electric field on the surface of the drops.

We note also that some authors reject the notion that the drop radius scales as $R_K$, in spite of the available experimental evidence.[19,20,22] This disagreement is a theoretical reflection of the perception that fluid inertia may become important in the jet region, whereupon the jet radius could depend also on the fluid density $\rho$ through the flow rate parameter $\eta$,

$$\eta^2\equiv\frac{\rho KQ}{\gamma\epsilon\epsilon_0}. \tag{8}$$

These refinements are, however, of minor relevance for the present task, since they involve multiplication by small powers of the quantity $\eta$, which is itself of order unity. Hence, the same data on mean drop diameter $\langle D_d\rangle$ which for Refs. 22 and 19 are proportional to $R_K$, appear also as approximately proportional to $R_K\eta^{1/3}$ when graphed by Ref. 24. In any case, inertia is negligible in the apex region, where we have just seen that the maximum electric field arises. The status of $E_K$ as the appropriate variable to describe field evaporation from the meniscus is therefore not affected by these subtle disagreements. For the time being we will use either $E_I$ or $E_K$ as alternative measures of the maximum electric field, $E_{\max}$ on the meniscus surface:

$$E_{\max}\equiv\varphi_I(\epsilon)E_I\equiv\varphi_K(\epsilon)E_K, \tag{9}$$

where the value of the proportionality coefficients $\varphi$ and their dependence on the dielectric constant remain to be determined either by theory or experiment. An approximate lower bound for $\varphi$ may be given from the condition that $E_{\max}$ exceeds the value of the field $E_j$ near the end of the jet, given from Eq. (3) for $R=R_j$. But $R_j$ is known experimentally to be given approximately by the most probable drop radius divided by 1.89,[25] very much as in the Rayleigh breakup of uncharged jets. Making use also of the scaling laws for the drop diameter and the jet current we may rewrite Eq. (3) particularized at $R=R_j$ as

$$E_j\sim\frac{F(\epsilon)G(\epsilon)}{4\times 1.89}E_K. \tag{10}$$

For the case of formamide, Chen and Pui[19] report data which imply that $F(\epsilon)=2.34$, $G(\epsilon)=3.84$, so that $E_j=1.19E_K$, giving the approximate lower bound

$$\varphi_K(111)>1.19. \tag{11}$$

The scaling law for the current may also be used to give the approximate relation $E_I/E_K=[F(\epsilon)]^{1/3}$. For the case of formamide, this leads to the approximate ratios:

$$E_I/E_K=\varphi_K/\varphi_I\sim 1.33. \tag{12}$$

Cherney's first order corrections to Taylor's field yields a maximum for the field in the near apex region of the cone.[21b] His results imply too low a value for $\varphi_K$ in the case of formamide, perhaps because his computed maximum is located too close to the apex region for the analysis to hold. The scaling Eq. (5b), however, is preserved in Cherney's work. In any case, except for an unknown multiplying factor of order unity, Eqs. (5a), (5b) provide suitable scales for the strength of the electric field in terms of the easily measured macroscopic quantities $K$, $Q$ and $I$. Pending future determination of $\varphi$ by either electron microscopic observations or numerical work, the present study will be based on controlling the surface electric field $E$ via the variables $Q$ and $K$, and will use the incomplete but quantitative measures $E_K$ and $E_I$ for its value.

### B. The electric field on the surface of the drops

The total ion current originating from the drops cannot exceed the current emitted by the jet in the form of drops. Furthermore, the net charge and surface electric field on an ion-evaporating drop decay in time. Hence, due to the steep dependence of the ionization rate on the field, the ion current from the drops will be at most a small fraction of the total drop current (say 10%). Another important difference between ion evaporation from the meniscus and from the drops is that the first process can modify the magnitude of the total spray current [given by Eq. (6) in the absence of ion evaporation from the cone-jet], while the second cannot. The reason is that the spray current is determined by electrohydrodynamic processes occurring in the meniscus, and cannot be modified by whether or not the drops evaporate some ions after the break-up of the jet.

In a problem where the ionization rate has such a steep variation with $E$, the maximum field is more relevant than the average field that could be constructed in terms of the mean drop charge and diameter. An upper bound for $E$ follows from the fact that the maximum charge on a drop of diameter $D_d$ must be smaller than the Rayleigh charge $q_R$:

$$q \leqslant q_R \equiv \pi(8\gamma\epsilon_0 D_d^3)^{1/2}. \tag{13}$$

Furthermore, the ratio of charge over volume for the drops produced from a given cone-jet is narrowly distributed around a mean value nearly equal to the ratio $I/Q$:[26,27]

$$q = \frac{\pi D_d^3}{6}\frac{I}{Q}. \tag{14}$$

For a given spray (fixed $K$, $Q$, and $I$), these two expressions establish the following upper bounds (involving only measurable quantities) for both the drop diameter and its surface field:

$$D_d \leqslant 3.3 R_I; \tag{15}$$

$$E_d \leqslant 1.1 E_I. \tag{16}$$

Notice that $I$ must be based on the current carried by the drops initially produced, and should therefore exclude the current of ions emitted directly from the jet (but not from the drops).

Two final remarks are in order regarding potential problems associated with the use of Eq. (16) to represent the actual maximum field on the drop surface. First, the upper bound found is approached provided only that some of the spray drops reach the Rayleigh limit, which does not always happen in electrosprays, particularly not near the minimum flow rate in moderately conducting solutions.[28] But the presence of such drops in the spray can be inferred directly (via stopping potential measurements; Sec. IV D) from the occurrence of in-flight Coulomb explosions. We will therefore be able to establish that for all the formamide sprays used in this work, *if they are spherical*, some of the drops do reach the limiting condition Eq. (14), so that the maximum field on the drop surface is actually given by the right hand side of Eq. (16):

$$(E_d)_{\max} = 1.1 E_I. \tag{17}$$

A second problem with the reasoning leading to Eq. (17) is that it takes the drop to be spherical. But the drop is not spherical at birth. Rather, it originates on the breakup of a cylindrical jet, which, in Rayleigh's theory for uncharged liquids has a length some nine times greater than its radius. This sausage-shaped fragment must initially have a field considerably larger in its polar region than that for a sphere with the same charge and volume, and a comparably smaller field on its cylindrical surface. Ion evaporation will hence occur first from the endpoints and, once the two polar regions have relieved themselves of excess charge, they will stop evaporating ions. The drop will then undergo several oscillations, during which the curvature in the equatorial region will periodically approach that of a sphere. Eventually the whole drop will become spherical after having dissipated its internal kinetic energy. During the initial nonspherical phase, although there is little rearrangement of net charge, the distribution of electric fields will be very close to that of a conducting drop due to the high dielectric constant of formamide and to the short times associated to polarization of the solvent. One could certainly undertake the exercise of computing the time dependent distributions of fields on this oscillating drop, to infer from them the total ionization current versus time. However, it is clear that this field will be represented by that on the final spherical drop, times a certain geometric factor $\varphi_s$ of the order one. The characteristic surface field inferred in Eq. (17) for a strictly spherical shape is therefore not exactly equal to the maximum field on the drop surface, very much as with the quantity $E_K$ used as a measure of the field on the tip of the meniscus. In spite of this unfortunate fact, pending a future numerical determination of $\varphi_s$, we shall provisionally proceed as if Eq. (17) were exact.

### C. A working fluid to create fields $E \sim 1$ V/nm in vacuum

A second factor which has hindered a direct measurement of the kinetics of ion evaporation has been the lack of a liquid suitable to form Taylor cones in vacuum while being also capable of providing sufficient electrical conductivities to reach the required strength $E_K \sim 1$ V/nm. High values of $K$ require high dielectric constants and moderate viscosity co-

TABLE I. Physical properties of formamide. $\rho$=density; $\mu$=viscosity coefficient; $\gamma$=surface tension; $p_0(T)$ vapor pressure.

| $\epsilon$ (20 °C) | $\rho$ (20 °C) (kg/m$^3$) | $\mu$ (20 °C) (kg m$^{-1}$ s$^{-1}$) | $\gamma$ (20 °C) (N/m) | $p_0$ (129.4 °C) (Pa) | $p_0$ (20 °C) (Pa) |
|---|---|---|---|---|---|
| 111.0 | 1133.4 | 0.003 764 | 0.0583 | 3960 | ~1.9 |

efficients. Yet, most liquids having such characteristics are too volatile for stable operation in a vacuum. The vast majority of published vacuum studies on Taylor cones of organic liquids have used glycerol heavily doped with salts. But the very high viscosity of this liquid is associated with small ionic mobilities and hence with electrical conductivities smaller than 0.05 S/m (a 19.3% solution by weight of NaI in glycerol has an electrical conductivity of 0.021 S/m).[29] The only report we know of a substance other than a liquid-metal leading to the evaporation of high currents of ions is for sulfuric acid.[13] This behavior corresponds clearly to a situation where the electrical conductivity is already too high ($K \sim 10$ S/m) for the transition between negligible to measurable ionic currents to be observable. Under these conditions, the scaling laws Eqs. (4)–(7) cannot be expected to hold.

Determining the appropriate range of electrical conductivities at which this transition would be capturable requires using not only Eq. (5b) with a value $E_K \sim 1$ V/nm, but also some information on the minimum flow rate $Q_{\min}(K)$ at which a stable Taylor cone may be formed with a liquid of given electrical conductivity. This point has been addressed in Ref. 18, with the conclusion that the group $\eta$ defined in Eq. (8) is generally comparable to unity. Substituting this criterion into Eq. (5b) with typical values for formamide, one finds that electrical conductivities in the range of 1.3 S/m are required. This estimate therefore fits the experimental observations already mentioned showing that glycerol solutions as well as sulfuric acid are both either too far below or above the range sought.

The present study will be based on formamide, the only solvent we know that can span the desired conductivity range and is sufficiently involatile to form a stable Taylor cone in a vacuum. Its physical properties are shown in Table I.[30] It dissolves alkali halide salts at concentrations above 1 M. Its nonnegligible evaporation rate from the meniscus surface can be made relatively unimportant by supporting the Taylor cones on micro-needles carefully tapered to a tip diameter of some 20 $\mu$m.

The concentration and the measured electrical conductivity and surface tension of the solutions studied are shown in Table II. Note that the name of the solution conveys information on its electrical conductivity. The magnitudes of $E_I$ and $E_K$ used are based on these quantities.

TABLE II. Characteristics of the solutions used in this study.

| Solution | Concentration of NaI (M) | Conductivity K (S/m) | $\gamma$ (22 °C) (N/m) |
|---|---|---|---|
| F02 | 0.10 | 0.21 (21 °C) | |
| F03 | 0.17 | 0.31 (21 °C) | |
| F07 | 0.50 | 0.71 (21 °C) | 0.0587 |
| F11 | 1.00 | 1.12 (21 °C) | 0.0595 |
| F14 | 1.50 | 1.42 (21 °C) | 0.0601 |
| F16 | 2.00 | 1.67 (21 °C) | 0.0609 |
| F22 | 3.00 | 2.20 (27 °C) | 0.0618 |

## III. EXPERIMENT

### A. Setup

The basic setup used in this study is shown in Fig. 2. The liquid to be sprayed was driven through a fused silica line (15 or 20 $\mu$m internal diameter, Polymicro Technologies, Inc., Phoenix, Arizona), from a glass reservoir containing the liquid solution, into the electrospray chamber. The end of the silica line supporting the liquid meniscus was sharpened into a cone and made conductive by deposition of a thin tin oxide film. The liquid reservoir pressure relative to the electrospray chamber was varied using a mechanical vacuum pump and pressurized $CO_2$. It was measured with a mercury manometer. For each liquid solution, a calibration curve (straight line) was constructed relating this pressure drop through the silica line and the flow rate. The chamber was connected through a valve to a turbomolecular pump forepump system, as well as to a controlled leak of $CO_2$. This allowed continuously varying the pressure from $10^{-5}$ Torr up to 1 Atm, as measured with an ion gauge, a MKS Baratron type 122A pressure transducer, or a mercury manometer.

Figure 3 shows the electrode arrangement used to perform stopping potential measurements of electrospray drops and ions. These measurements are carried out by fixing the voltage difference between the needle and the extractor (to fix the cone structure) while keeping the collector at ground. One then sweeps over the voltage difference between the needle and the collector by varying the extractor voltage. Occasionally a fourth piece, referred to here as ''the lens,''

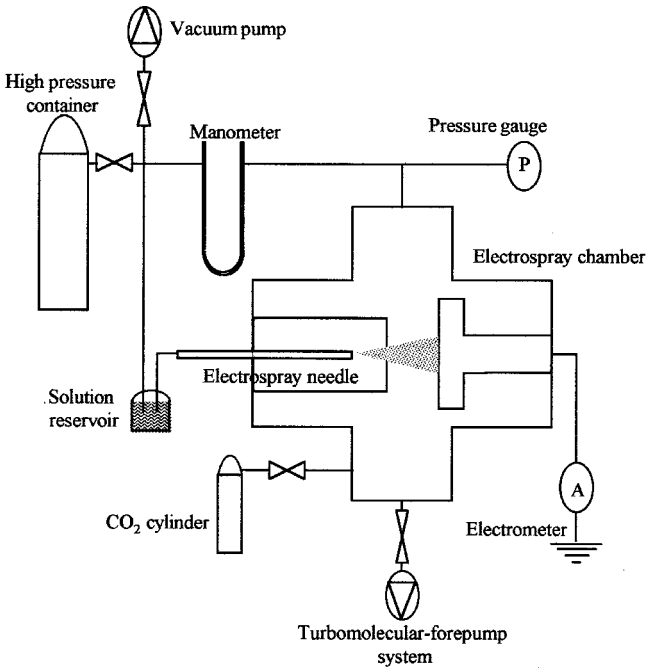


FIG. 2. Experimental setup.

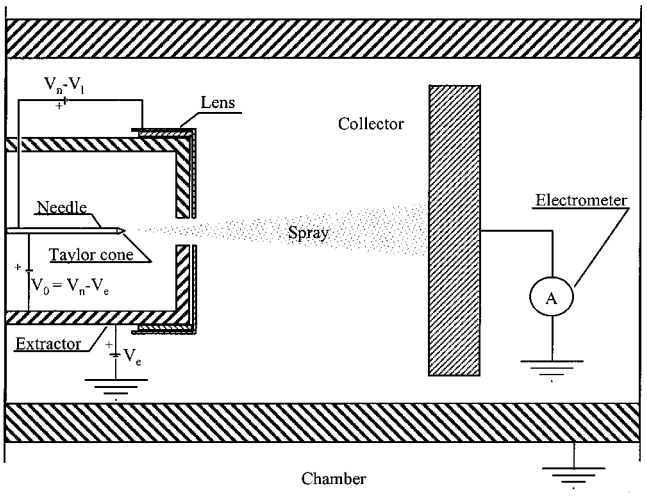


FIG. 3. Electrode geometry within the electrospray chamber.

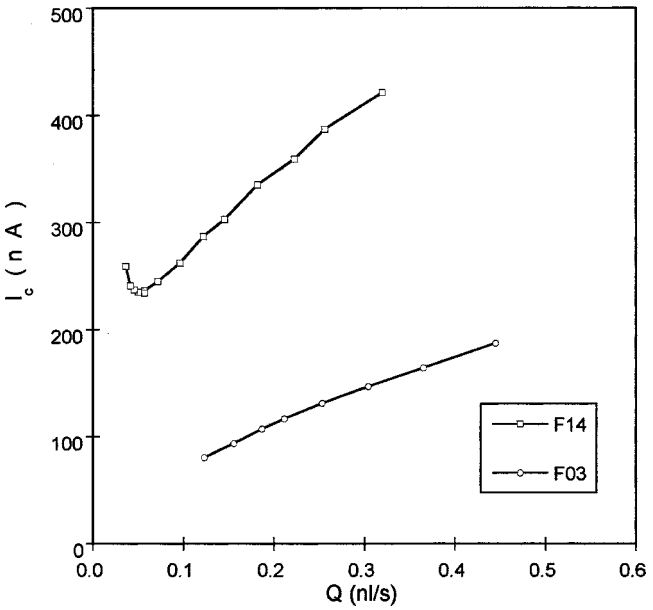


FIG. 4. Typical electrospray current versus liquid flow rate for solutions F14 and F03. The anomalous increase in current observed below a critical flow rate for F14 is attributed to the onset of ion evaporation.

was used to control the field ahead of the collector independently of the extractor potential. The electric currents reaching each electrode as well as their respective voltages referred to the collector were measured, and their values taken to a computer.

### B. Measurement technique

The appearance of a qualitative change in the behavior of Taylor cone-jets when the characteristic field $E_K$ reaches values of the order of 1 V/nm is readily detected by measuring the spray current $I$ as a function of liquid flow rate $Q$. Increasing the electrical conductivity and decreasing $Q$ under atmospheric conditions, one eventually strikes a mild electrical discharge. This behavior will be discussed in Sec. IV F, but provides a first indication that ions are released at substantial rates from the liquid surface. The same observation may be made far more quantitatively under a vacuum, as seen in the rather different behavior of the $I(Q)$ curves shown in Fig. 4 for two formamide solutions, F03 and F14. The lowest $Q$ values included correspond in both curves to the minimum flow rate at which a stable cone-jet forms. The background pressure was 30 mTorr and the extractor faced the collector directly, without the intermediate lens. The extractor was biased 20 V positive, relative to the earthed collector (no secondary electron suppression in this case). The collector current decreases monotonically with the flow rate for the solution with lower conductivity, as expected from Eq. (6). The current for F14 behaves quite similarly at large flow rates, but goes through a previously unreported minimum at a critical flow rate $Q^* = 0.057$ nl/s. Interestingly, the corresponding value of $E_K$ is 0.96 V/nm, in the expected range for the onset of ion evaporation. It is therefore natural to attribute the increase in total current arising at $Q < Q^*$ to the fact that the field on the meniscus surface has reached the critical value required for ion evaporation, and this process becomes more intense at diminishing flow rates because $E_K$ increases further. This interpretation is strengthened by the fact that the minimum in the current appears only above a critical electrical conductivity. Indeed, below a critical $K$, $E_K$ would remain below the required critical field, even at the minimum flow rate. Solution F03 exhibits this more familiar subcritical behavior in Fig. 4.

A negative current (not plotted in Fig. 4) was also measured at the extractor. Its value was $-6$ nA for solution F02 and $-20$ nA for solution F14 (in this last case the negative current also increased below $Q^*$). Because the needle is raised to a positive voltage, the appearance of negative currents indicates that electrons are emitted inside the chamber by secondary effects. Because the charge-to-mass ratio of the electrospray drops is far too small to produce secondary electrons at impact energies of a few kV, these electrons provide still another indication that substantial ion currents evaporate from the liquid. Our task now is to isolate the current originating in the liquid surface in the form of ions from current carried by drops and secondary ionization processes.

First, we can be sure that the ionic current measured is not magnified by secondary ionization due to collisions of the primary ions with neutral gas molecules. This multiplication, if present, would proceed principally in the region between the needle and the extractor, where the background pressure is highest (the source of formamide vapors is right there). We are sure that no ions impinge on the extractor surfaces facing the needle, since no measurable electric current reached this electrode in any experiment with the lens charged to the same potential as the extractor. Volume ionization can also be rejected because the electric current $I_n$ measured in the needle did not vary when the background pressure changed from 0.02 mTorr to 40 mTorr. Notice that this includes pressures higher than the vapor pressure of formamide, estimated to be 14 mTorr.[30] This experiment was executed with solution F14, at flow rates below and above $Q^*$.

Let us now consider the zone lens collector under the conditions of Fig. 3, with a stable cone-jet at $V_0 = 1479$ V

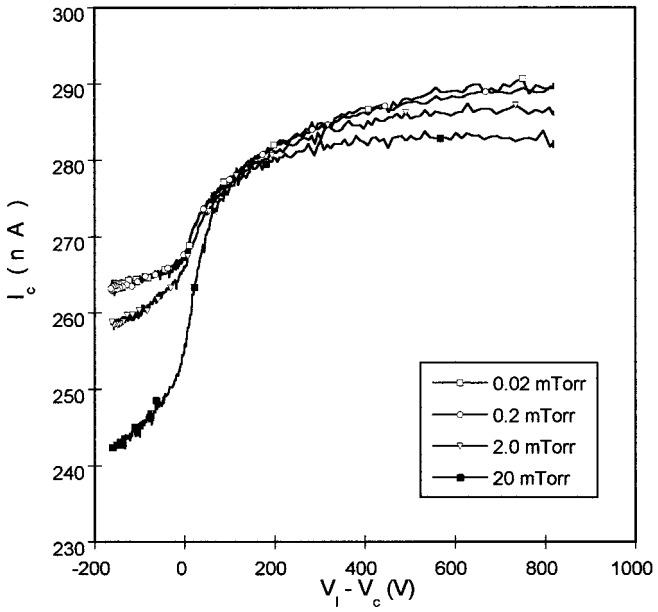


FIG. 5. Dependence of the stopping potential curves on background pressure and electric field in the lens collector zone.

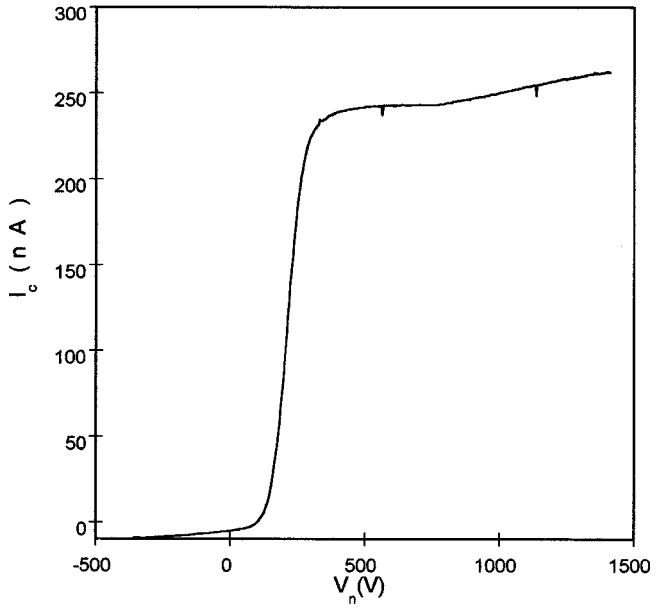


FIG. 6. Stopping potential curve for solution F14, $Q=0.061$ nl/s. The constant value of the current measured in the collector during the interval $400<V_n<800$ corresponds to the current emitted by the cone-jet.

above the extractor. The extractor is kept at the same potential as the lens ($V_l$), which is varied with respect to the grounded collector to create an electric field, $E_x$, between the lens and the collector. In this situation, the current measured in the collector, $I_c$, is the sum of the primary current (the whole spray coming from the Taylor cone reaches the collector) and the secondary current generated in this region (the sign of this one depends on the direction of $E_x$; $E_x$ is positive when the lens voltage is also positive). Figure 5 plots curves of $I_c$ versus the difference $V_l-V_c$ between lens and collector voltage, for a fixed flow rate of solution F14 at several background pressures, covering three orders of magnitude. Ion-neutral collisions are highly improbable at the lowest pressure, 0.02 mTorr, when the gas mean free path is some 2.5 m. However $I_c$ does depend on $E_x$, especially for positive $E_x$. Accordingly, in this case the secondary current must be due to ejection of electrons from the collector surface by impact of the positive ions (note that a smaller amount of positive particles could be released as well). This current is positive because the negative electrons are released from the collector and flow to the lens following the electric field. When $E_x$ is negative the situation changes: now electrons are equally released but they return to the collector, leading to a smaller variation of $I_c$ with $E_x$. The curves for 0.2 mTorr, 2 mTorr and 20 mTorr are quite similar for positive and moderately large $E_x$. The gas mean free path for the highest pressure is 2.5 mm and several collisions will now occur. However, $I_c$ does not change substantially and, in any case, decreases, while the opposite would happen if volume ionization were the source of electron emission. One then concludes that secondary ionization originates mainly due to surface collisions at the collector.

Notice also in Fig. 5 that $I_c$ decreases substantially at high enough pressures and negative (or small) $E_x$. We shall attribute this behavior to the fact that the least massive particles in the spray are stopped by collisions with the background gas, and then follow the electric field lines, either into the lens or the collector depending on the sign of $E_x$. Given the large mass disparity between ions and the smallest drops present in the spray, it is possible to fix the pressure such that all ions but none of the drops are stopped, thus providing a simple means to measure the ion current independently from that associated with the drops. The possible contribution to these steps of secondary phenomena associated to ion-neutral collisions at 10 or 20 mTorr could raise concerns here. Notice, however, that the probability of ion-neutral collisions cannot change drastically when the field between extractor and collector vanishes, and such phenomena cannot therefore account for the observed steps.

The measurement routine to infer the total current and the ion current is as follows:

*I*: The total current is measured at the collector at the lowest background pressure, with a negative electric field between lens and collector. The lens acts here as the standard ''suppressor'' of secondary electrons. This point is illustrated in the stopping potential curve shown in Fig. 6 for solution F14, for a liquid flow rate of 0.061 nl/s. The current measured in the collector is plotted as a function of the voltage difference between needle and collector, $V_n$, with the geometric configuration of Fig. 3 (we keep constant the voltage difference between needle and extractor, $V_0=V_n-V_c=1489$ V, and between needle and lens, $V_n-V_l=800$ V, while the collector is grounded and the extractor potential is varied). When $V_n$ is small, the particles generated in the cone-jet do not have enough energy to reach the collector and impact in the lens. Here, some electrons are released and reach the collector as a negative current following the electric field, $E_x$. As $V_n$ increases, the spray reaches the collector increasingly and eventually $I_c$ reaches an asymptote. Now the ions impact on the collector, but no electrons escape because $E_x$ forces them back to the collector. At this point, $I_c$

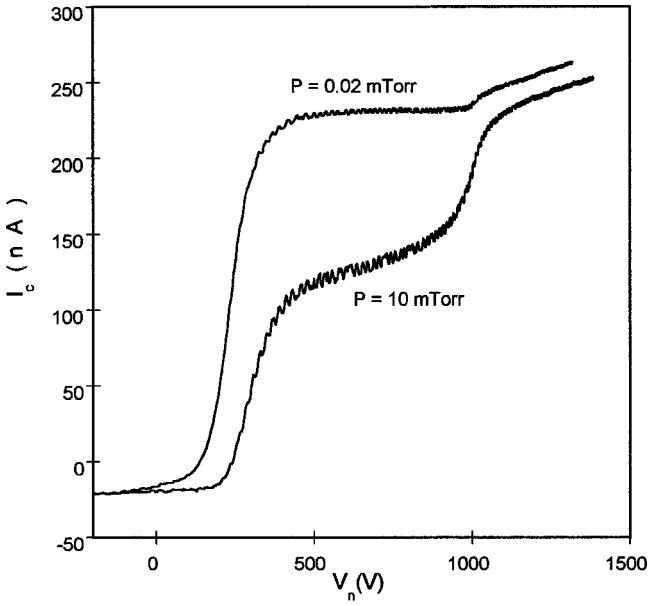


FIG. 7. Stopping potential curves for solution F16 ($Q=0.031$ nl/s) taken at background pressures of 0.02 mTorr and 10 mTorr. In the second case collisions with gas molecules stop the ionic fraction of the electrospray and allows its determination.

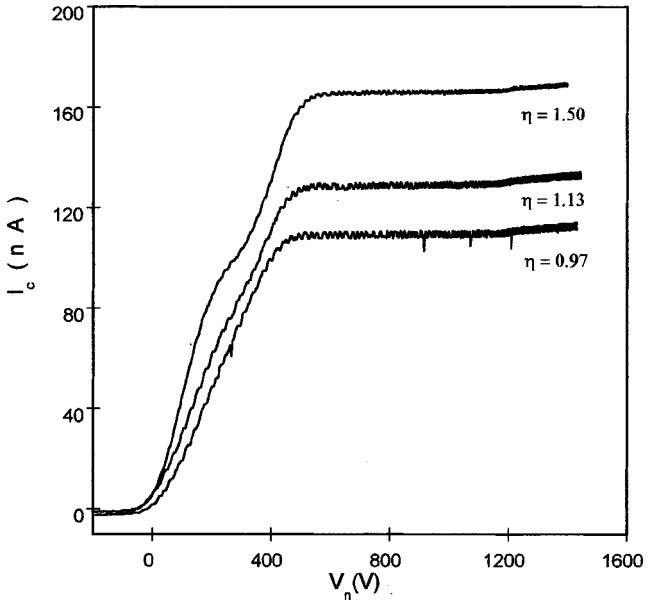


FIG. 8. Stopping potential curves for solution F07 at 0.02 mTorr of background pressure. The two-step structure observed at intermediate flow rates is due to in-flight Coulomb fissions. Their suppression at the smallest flow rate is attributed to ion evaporation from the drops.

corresponds to the total current emitted by the cone-jet, as confirmed by the fact that no charge reaches either the lens or the extractor. After $E_x$ changes its sign ($V_l=0$, or equivalently, $V_n=800$ V), $I_c$ is no longer constant and increases due to electron emission.

$I_i$: The ion current is inferred from the step appearing in $I_c$ when the sign of $E_x$ changes at a background pressure in the right range to stop all the ions but none of the drops. This is illustrated for solution F16 in the stopping potential curves of Fig. 7, taken at two background pressures ($Q=0.031$ nl/s; $V_0=1489$ V: $V_n-V_l=1000$ V). The curve taken at 10 mTorr resolves two types of particles. One of them loses a little energy but reaches the collector similarly as under low background conditions (0.02 mTorr). The other is completely stopped by the background gas, and then drifts through it in the direction of the electric field. It can thus reach the collector only when $V_l>V_c$, as indicated by the step at $V_n=1000$ V.

An inherent danger in the interpretation of these measurements is associated to the fact that cone-jets often emit two types of drops, generally referred to as primaries and satellites. Since the satellites have masses considerably smaller than the main drops they would also be stopped first. However, we can unambiguously determine the conditions required to stop these satellites and verify that they differ drastically from those at which ions are stopped. The phenomenon of in-flight Coulomb explosion arising in electrosprays is known to produce drops of satellite dimensions.[22] Their appearance can be induced or suppressed by increasing or decreasing the liquid flow rate through the cone-jet.[28] Furthermore, these drops are distinguishable from the main drops because they produce a second step at considerably lower energy in the stopping potential curves. Figure 8 is for solution F07 at a background pressure of 0.02 mTorr. It shows stopping potential curves exhibiting this double step (hence involving satellite drops) clearly at $\eta=1.5$, marginally at 1.13, but not at the smallest flow rate, $\eta=0.97$. Figure 9 illustrates the dependence of the stopping potential curves on the background pressure for the lowest flow rate, at which there are no Coulomb explosions. Figure 10 is similar to Fig. 9, but now some daughter drops are produced in Coulomb fissions. These satellites are clearly much more massive than the ions because, even though they lose more energy than the primary drops as a result of their collisions with the gas, they are not stopped even at a background pressure of 25 mTorr.

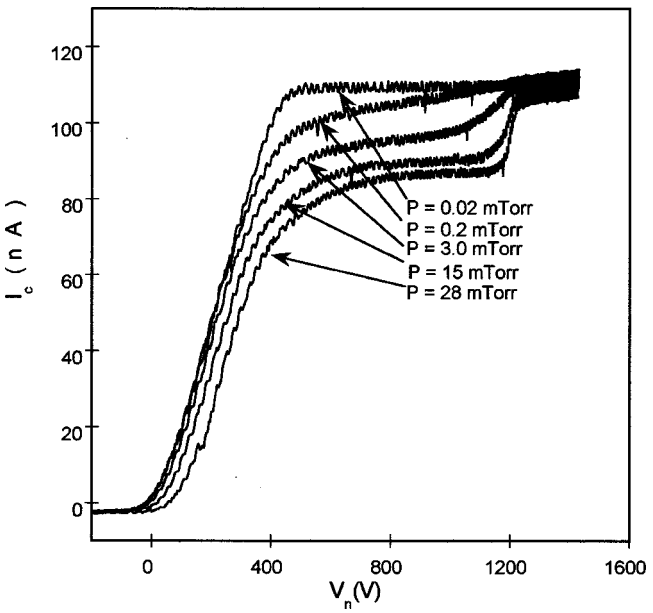


FIG. 9. Stopping potential curves for solution F07 at different background pressures ($\eta=0.97$).

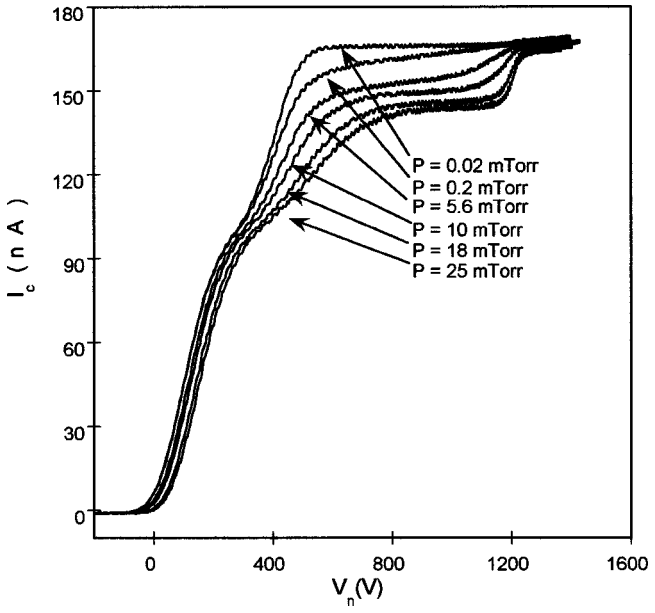


FIG. 10. Stopping potential curves for solution F07 at different background pressures ($\eta$=1.50).

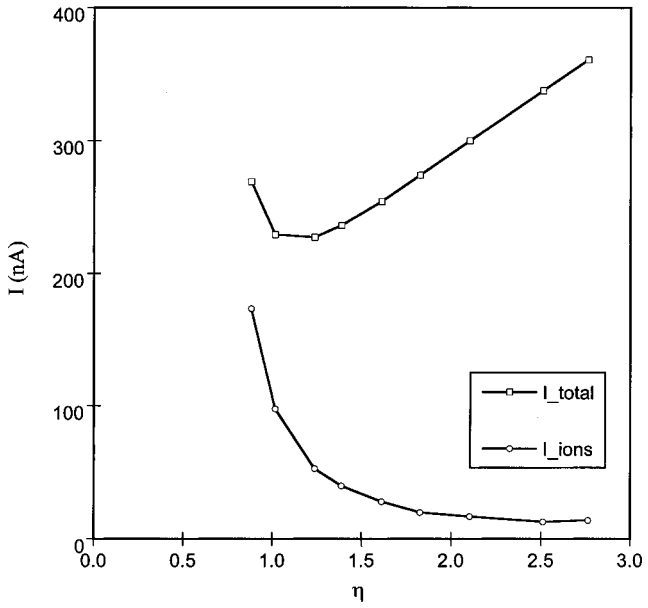


FIG. 12. Total and ion currents for solution F16.

In contrast, almost all the ions are stopped at some 10 mTorr both in Fig. 9 and Fig. 10. Accordingly we will set a background pressure of 10 mTorr as a reasonable value to separate the ions from the drops.

## IV. IONIZATION CURRENT

### A. Total current from the Taylor cone

Figure 11 shows the total current (drops+ions) measured at 0.02 mTorr, as described in Sec. III B. In order to make the horizontal scale cover the same range of values at all electrical conductivities, we use the dimensionless flow rate parameter $\eta$ ($\sim Q^{1/2}$) defined in Eq. (8) instead of $Q$. The various curves drawn are for formamide solutions with increasing conductivities. The behavior is analogous to that in Fig. 4. Both $\eta$ and the flow rate at the minimum of these curves increases with liquid conductivity ($Q=0.0417$ nl/s, $Q=0.0458$ nl/s and $Q=0.0556$ nl/s for F14, F16 and F22, respectively). This is to be expected, since the electric field and hence the ratio $K/Q$ should be approximately constant at the minimum.

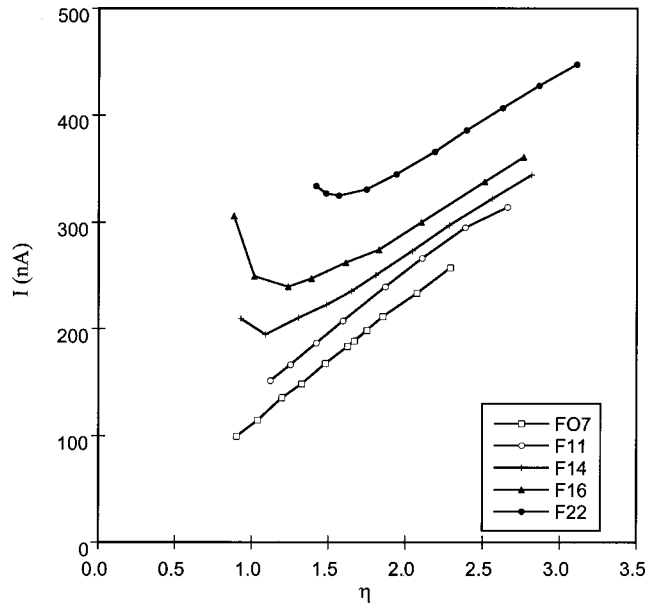


FIG. 11. Current versus flow rate parameter for several formamide solutions. The most conducting ones exhibit a minimum associated to the onset of ion evaporation below a critical flow rate.

### B. Ion evaporation from drops in flight

The anomalous minimum observed in Fig. 11 for several $I(Q)$ curves cannot be due to ion evaporation from drops in flight, because, in the absence of ion evaporation from the cone-jet, the spray current is fixed prior to jet breakup and would vary monotonically with $Q$. Nonetheless, the field on the drops exceeds that on the meniscus, and a certain fraction of the observed ion current will therefore originate from the drops. A rather direct proof that charge is in fact evaporating from droplets in flight can be derived from the suppression of Coulomb explosions at a sufficiently high $K/Q$ ratio, as already observed at the lowest flow rate of F07 in Fig. 8. This phenomenon will be investigated further in Sec. IV D.

Figure 12 plots the total and ionic currents for solution F16 versus the flow rate parameter $\eta$. Some of the raw stopping potential curves leading to these data are shown in Fig. 13, exhibiting a dramatic shift from drop current (first step) to ion current (second step) at diminishing $\eta$. Notice three regions in the ion current curve in Fig. 12. It appears to asymptote to a nonzero value at large flow rates ($\eta>2.5$), increases moderately down to the vicinity of the minimum in the total current ($2.5>\eta>1.2$), and finally increases far more rapidly below $\eta=1.2$. We shall argue that the ions produced in the intermediate region ($2.5>\eta>1.2$) originate on the drops, with negligible contributions from the jet. This current rises first rapidly at decreasing flow rates [hence increasing

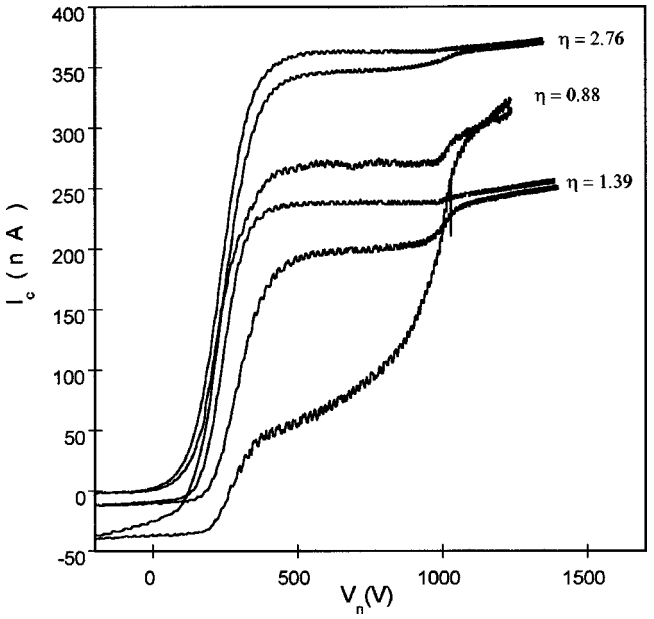


FIG. 13. Stopping potential curves for solution F16, at different flow rates. The ion current for each flow rate is inferred from the difference between $I_c$ at 0.02 mTorr and $I_c$ at 10 mTorr.

field $E_I$ in Eq. (5)], but its growth becomes soon much slower because the drops have a finite supply of charge, and can only evaporate a limited portion of it before the electric field on their surface decays below the necessary level. Eventually, for even lower flow rates, the field becomes large enough for ions to evaporate directly from the meniscus. This final process can dominate the picture even though $E_{\text{jet}}<E_{\text{drop}}$, because the jet is directly connected to the power supply, and is hence free from the saturation mechanism limiting the ion current from the drops.

This qualitative reasoning may be made quantitative by use of an explicit expression for the ion evaporation rate,[7] essentially based on that given by Iribarne and Thomson:[5]

$$j''=\frac{kT}{h}\sigma\exp\left[-\frac{\Delta G_s^0-G_E(E)}{kT}\right], \tag{18}$$

where $j''$ is the flux of evaporating charge ($\mathrm{C\,m^{-2}s^{-1}}$), $\sigma$ ($\mathrm{C\,m^{-2}}$) is the surface charge density, $h$ is Planck's constant, $\Delta G_s^0$ is the activation energy for ion evaporation in the absence of electric field, and $G_E(E)$, already introduced in Eq. (1), is the reduction of this activation barrier due to the field. For the case of a spherical drop holding a total number of charges $z(t)$ and keeping a (constant) radius $R$, charge conservation and Eq. (18) are used to obtain

$$\frac{d\Psi}{dt}=-A\frac{d\Psi}{d\ln z}e^{\Psi}; \tag{19}$$

$$A=\frac{kT}{h}\exp\left[-\frac{\Delta G_s^0}{kT}\right]; \tag{20}$$

$$\Psi=\frac{G_E(E)}{kT}, \tag{21}$$

where $A$ is a constant frequency factor, and $\Psi$ is chosen as the new dependent variable because it appears in the exponent and dominates the picture once it has reached a certain critical value. When $G_E(E)$ is given by Eq. (1),

$$\frac{d\Psi}{d\ln z}=\Psi/2. \tag{22}$$

This expression is adequate for relatively large drops of liquids with high dielectric constant.[7] In any case, $d\Psi/d\ln z$ is a slowly varying function of $\Psi$ which may be taken as constant at the scale of the rapid variation of the $e^{\Psi}$ term. Whatever the specific dependence $d\Psi/d\ln z=\Lambda(\Psi)$, Eq. (19) may be reduced to a quadrature, and then integrated asymptotically in powers of the large parameter $1/\Psi_0$.[31] For the special case of Eq. (1), we find with errors of order $1/\Psi_0$:

$$e^y-1=\frac{At}{2}\Psi_0\exp[\Psi_0], \tag{23}$$

where $\Psi_0$ is the initial value of the exponent (at $t=0$) and its final value is $\Psi_0-y$:

$$y(t)=\Psi_0-\Psi(t). \tag{24}$$

Also with relative errors of order $1/\Psi_0$ the fraction of the drop charge lost as ions is:

$$\frac{z_0-z}{z_0}=\frac{\Delta z}{z}=\frac{2y}{\Psi_0}, \tag{25}$$

which is directly measurable as the fraction of the initial drop charge evaporated as ions:

$$\frac{\Delta z}{z}=\frac{\text{ion current from drop}}{\text{total drop current}}. \tag{26}$$

Equation (23) is therefore verifiable, since $y=\Psi_0\Delta z/(2z)$ is known experimentally from the measured currents, and $\Psi_0$ depends only on the electric field on the drop surface, which is $E_{\max}$, as given in Eq. (17) in terms of the measurable ratio $Q/I$:

$$\Psi_0=\frac{e^{3/2}}{2^{2/3}(\pi\epsilon_0)^{1/2}kT}\frac{(\gamma I)^{1/6}}{Q^{1/6}\epsilon_0^{1/3}}. \tag{27}$$

Equation (23) shows that $y$ depends exponentially on $\Psi_0$ at small $y(2y\sim At\Psi_0\exp[\Psi_0])$, so that:

$$\Delta z/z=At\exp[\Psi_0];\quad y\ll 1. \tag{28}$$

Figure 14(a) represents $\Delta z/z$ [as defined in Eq. (26)] versus $\exp[\Psi_0]$ for the points corresponding in Fig. 12 to the four largest flow rates. One sees indeed the initial linear behavior predicted by Eq. (28), which slows down considerably when $y$ ceases to be small. Indeed, at larger values of $\Psi_0$ when $y\gg 1$, both sides of Eq. (23) are dominated by their respective exponential terms, so that $y$ increases approximately only as a power of $\Psi_0$. The initial slope of $1.03\times10^{-25}$ fixes the group $At$, and hence the activation energy if $t$ is known. We estimate an available time of 1 ns (Sec. IV D), leading to $\Delta G_s^0=1.70\,\mathrm{eV}$. An error of one decade in $t$ leads only to an error of $kT\ln 10\sim 0.057\,\mathrm{eV}$ in $\Delta G_s^0$. It is pointless to refine this estimate given the comparable ambiguity in the normalizing current, since only a small fraction (from a few percent to some 10%) of the total current is initially associated to drops near the Rayleigh limit.

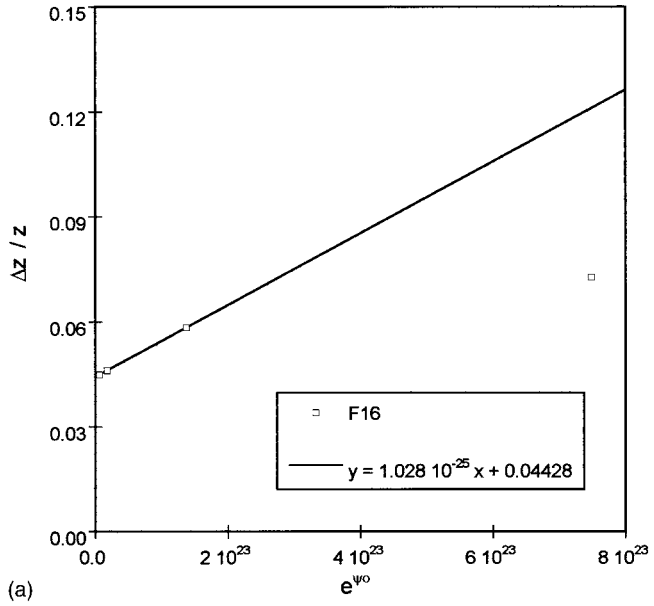


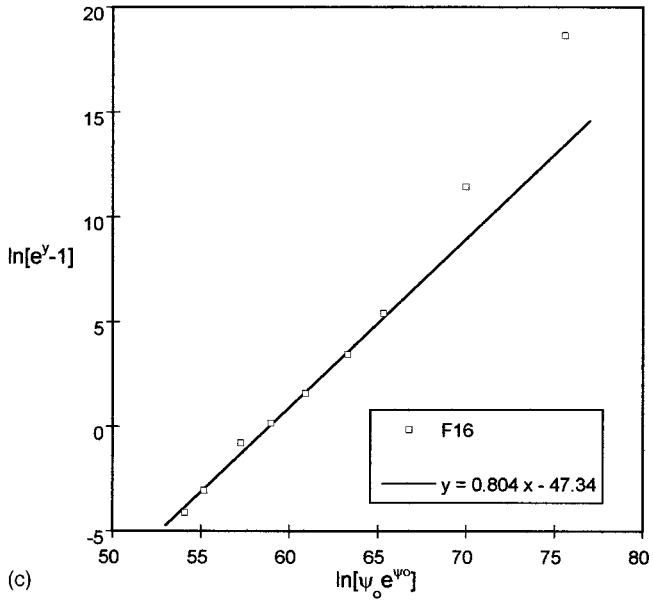


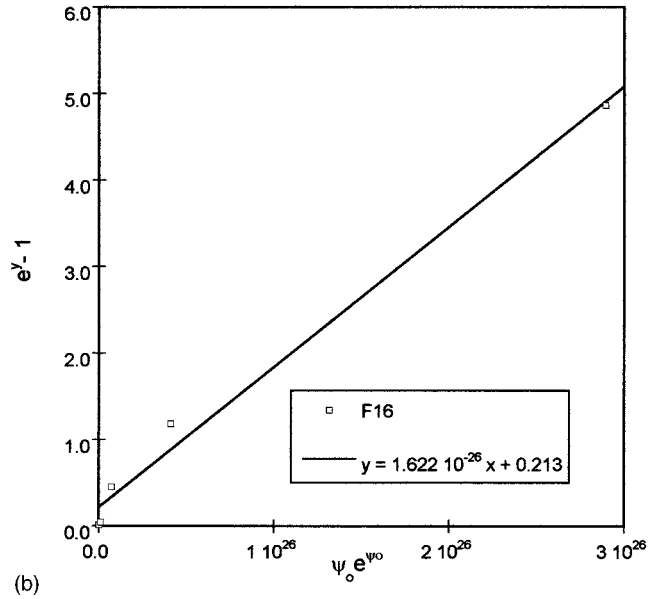


FIG. 14. Various representations of the ion evaporation current of Fig. 12 for solution F16. (a): plot of $\Delta z/z$ vs $\exp[\Psi_0]$ [Eqs. (26), (27)] for the four larger flow rates. Initially, the ion yield is linear with $\exp[\Psi_0]$. (b): plot of $(e^y-1)$ vs $\Psi_0 \exp[\Psi_0]$ [Eqs. (23), (24)] for intermediate flow rates. The ion evaporation from the drops saturates. (c): plot of $\log[e^y-1]$ vs $\log[\Psi \exp(\Psi_0)]$ for all flow rates in Fig. 12. Ions evaporate directly from the liquid meniscus for the three lowest flow rates.

An unexpected feature of Fig. 14(a) is that it extrapolates at small $\exp[\Psi_0]$ to a finite rather than a null ion current. This trend was already obvious in the finite ion current seen in Fig. 12 at large flow rates. The behavior is qualitatively the same for all the solutions studied, with a residual ion current which increases with electrical conductivity.[32] The most reasonable explanation for this phenomenon is that a small fraction of the liquid surface must exhibit curvatures and fields larger than those determined for the main drops. A possible location of such high curvatures is the polar region of the initially sausage-shaped detaching drop previously described. Another is the surface of small satellite drops generally produced together with the main drops at the jet breakup (or in Coulomb explosions). The diameters of these satellites may be several times smaller than the main drops.[22,33] de Juan[34] has analyzed superficially their charge, which is also a fair fraction of the Rayleigh limit. Hence, the electric fields on these satellites must be considerably larger than those for the main drops. However, because they only carry a small fraction of the spray current, they can only produce an even smaller current of ions. It is therefore natural that this contribution would have essentially reached its saturation value when the main drops begin to evaporate ions. Our data analysis will hence subtract a constant value to the quantity $\Delta z/z$, determined by a linear extrapolation such as the one which fixes that shift at $[\Delta z/z]_0=0.0443$ in Fig. 14(a).

In order to capture the behavior at larger values of $\exp[\Psi_0]$, at which $y$ is no longer small and the ion current begins to saturate, we represent it in Fig. 14(b) for solution F16 in the form $(e^y-1)$ vs $\Psi_0 \exp[\Psi_0]$, where the residual current $[\Delta z/z]_0=0.0443$ has now been subtracted. The figure contains only some of the lower points, since their values grow exponentially and cannot be represented in a linear plot. This representation gives also a closely linear fit, whose slope yields $At/2=1.62\times10^{-26}$. The corresponding value of $A$ is 3.1 times smaller than the one obtained in Fig. 14(a), but this difference leads to a negligible variation of the activation

TABLE III. Typical parameters governing ion evaporation from drops.

| Solution | At[a] | $[\Delta z/z]_0$ | At[b] | $\Psi_{0\ \min}$ | $\Psi_{0\ \max}$ | $\Delta G_s^{0a}$ | $\Delta G_s^{0b}$ |
|---|---|---|---|---|---|---|---|
| F22 | $1.03E-26$ | 0.111 | $8.77E-27$ | 52.3 | 64.7 | 1.75 | 1.75 |
| F16 | $1.03E-25$ | 0.044 | $3.24E-26$ | 50.1 | 71.3 | 1.70 | 1.70 |
| F14 | $7.99E-25$ | 0.033 | $1.21E-25$ | 48.1 | 63.9 | 1.65 | 1.69 |
| F07 | $4.78E-22$ | 0.026 | $5.48E-22$ | 43.7 | 50.9 | 1.50 | 1.50 |

[a]From linear fit at small $y$.
[b]From $e^y-1$ vs $\Psi_0 \exp[\Psi_0]$ curve.

energy. Hence, both the small $y$ as well as the large $y$ regions of these data yield the expected behavior.

Figure 14(c) is a log–log version of Fig. 14(b), now representing the full set of ionization currents. A linear best fit gives a slope smaller than unity, contrary to what would be expected. This could be interpreted as due to the fact that the exponent should not be $\Psi_0$, but $\varphi^{1/2}\Psi_0$. $\varphi$ would then be the square of the slope obtained. This interpretation would indicate that the assumption of $\varphi=1$ for the drops is too high, with a real value perhaps as small as 0.8. However, a value of $\varphi$ smaller than one appears as unphysical because a nonuniform field should lead to a maximum value larger than the mean. We note also that the linear fit found in Fig. 14(b) gives an equally satisfactory representation of the data in Fig. 14(c), while forcing its slope to be unity. The differences in slope found between these two fits may hence be physically irrelevant, perhaps due merely to the excessive weight assigned in log–log variables to the smallest values of $y$, which are very sensitive to the choice of $[\Delta z/z]_0$. In any case, these two graphs give us assurance that the choice of $\varphi=1$ implicit in Eq. (17) for the drops cannot be too far off.

The last three data points in Fig. 14(c) depart clearly from the general earlier linear trend, corresponding to conditions for which the total spray current approaches the minimum in Fig. 12 and goes beyond it. The excess current is clearly due to ion evaporation from the meniscus, and will be analyzed in Sec. IV C.

A similar data analysis for solutions F22, F14 and F07 yields an analogous behavior, with the main fitting parameters being collected in Table III. The behavior of F22 is shown in Figs. 15(a)–15(c). The residual current $[\Delta z/z]_0$ increases with solution conductivity, ranging from 1 nA for F02 to 40 nA for F22, with no significant dependence on the flow rate. Even though the changes in the various frequency factors are vast, the corresponding variations in the activation energies from one solution to the other are modest, except perhaps in the case of the least conducting one. The slightly anomalous behavior of F07 is likely associated to the small corresponding values of $\Psi_0$ (Table III). Consequently, it is possible that the residual current attributed to satellites drops may not yet be saturated in the case of F07, so that much of the change of ionization rate with $Q$ would not be due to the main drops, as assumed.

The activation energy found for a formamide-vacuum interface, $\Delta G_s^0=1.7$ eV, is considerably smaller than the accepted value 2.2–2.4 eV for the evaporation of $Na^+$ from the interface between water and its vapor.[35]

### C. Ion evaporation directly from the meniscus

The excess ion current observed in Figs. 14(c) and 15(c) over that originating in the drops is clearly due to ion evaporation from the meniscus. These two sources of ions may be separated by assuming that those coming from the drops would fall on the extrapolated straight line fit in the figure, the balance being assigned to ion evaporation from the meniscus. Notice that the $\Psi_o$ values for the last three points in Figs. 14(c) and 15(c) are incorrect, since the electric field Eq. (17) must be based on the total spray current minus the current of ions evaporated from the meniscus. This correction has been incorporated into the data of Fig. 16, where we plot drop current versus flow rate in dimensionless variables for several formamide solutions. Only the ion current emitted from the jet is subtracted from the full spray current, since that originating in the drops is part of the jet current.

In Fig. 17 we plot raw data of ion currents from the meniscus versus the electric field variables $E_I$ and $E_K$ defined in Eqs. (5a), (5b). All six curves exhibit a sharp rise in ion yield above similar characteristic electric fields $E_I \sim 1.5$ V/nm, $E_K \sim 1$ V/nm. Using the lower bound Eq. (11) for $\varphi_K$, the threshold electric field for ion evaporation from the meniscus would exceed 1.2 V/nm. Comparable values have been inferred at atmospheric pressure for tetrabutyl ammonium ions in water, ($E \sim 1.0$ V/nm),[34] and tetraheptyl ammonium ions in formamide ($E \sim 1.17$ V/nm).[36] It would be difficult to explain the qualitative features observed in Fig. 17 by a mechanism other than ion evaporation.

A more quantitative comparison between theory and the data of Fig. 17 has been attempted by integrating Eq. (18) over the meniscus surface while approximating the surface charge density as $\epsilon_0 E=\varphi_s \epsilon_0 E_s$. Here subscript $s$ refers to the scaling laws based either on the electrical conductivity ($S=K$) or the jet current ($S=I$). Computing the surface integral requires knowledge of the geometry and the distribution of $E$. Lacking this information, we have taken this integral to be given by the value of the integrand particularized at the point of maximum $E$ times an effective emission area, which we take to be equal to $R_s^2$ times a constant $\delta$ of order unity.

$$I_i=\delta\varphi_s\epsilon_0 E_s R_s^2 \frac{kT}{h}\exp\left[-\frac{\Delta G_s^0-(e^3\varphi_s E_s/4\pi\epsilon_0)^{1/2}}{kT}\right]. \tag{29}$$

Defining a function $\Psi$ for the exponent similarly as in Eq. (22),

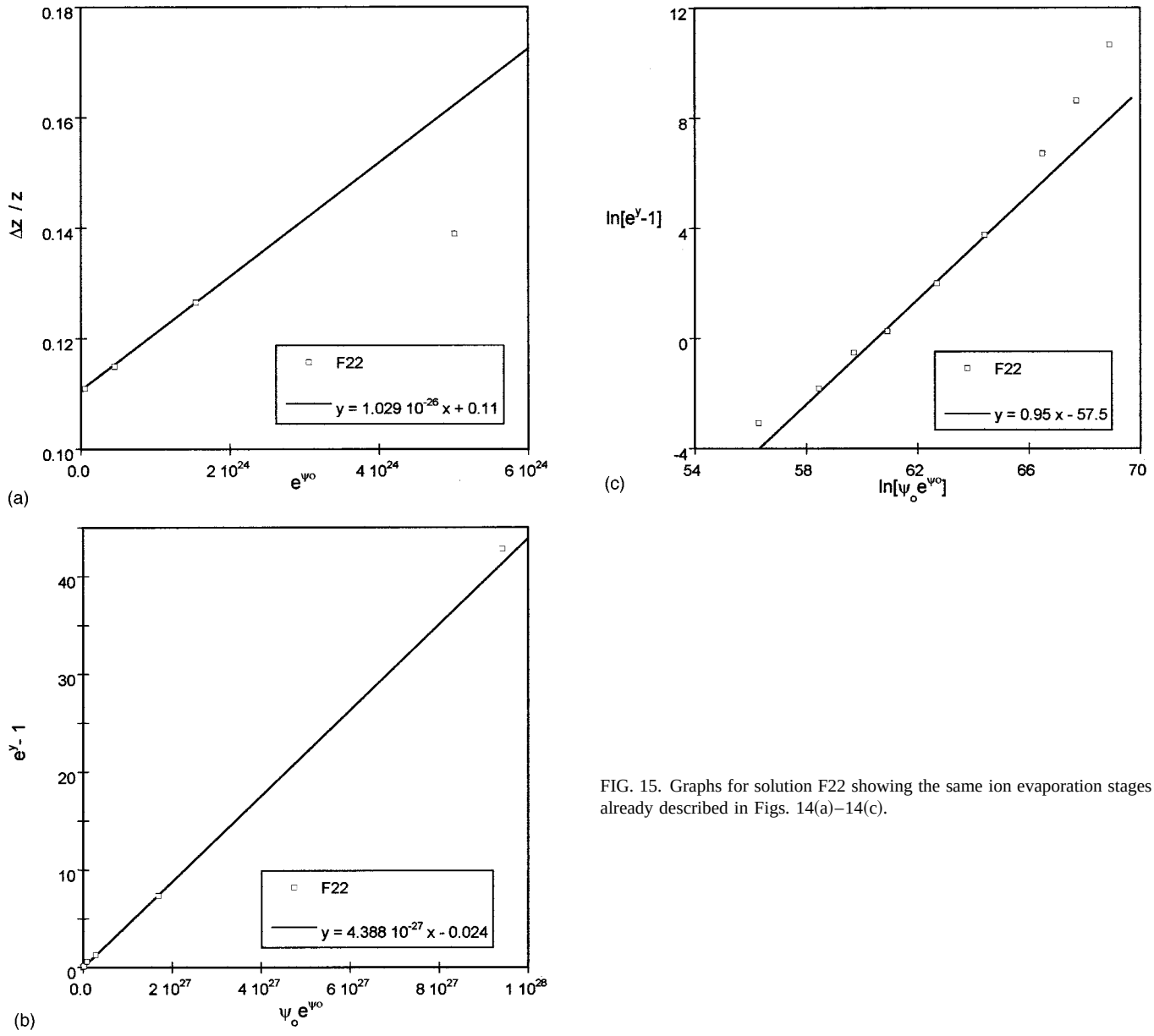


FIG. 15. Graphs for solution F22 showing the same ion evaporation stages already described in Figs. 14(a)–14(c).

$$\Psi_j = \frac{(e^3 E_s / 4\pi\epsilon_0)^{1/2}}{kT}, \tag{30}$$

we use the fact that $E_s R_s^2 = 4\gamma Q/I$ to show that the pre-exponential factor in the right hand side of Eq. (29) is proportional to $\Psi_j^{-6}$. Hence, a plot of $\ln[I_i \Psi_j^{-6}]$ vs $\Psi_j$ should give a straight line whose slope and intersection with the vertical axis determine the constants $\varphi_s$ and $\Delta G_s^0$ (except for the unknown value $\delta$). These plots yield indeed reasonably straight lines, but the associated regression analysis has too much scatter to provide reliable values for either $\varphi$ or $\Delta G_s^0$. For instance, putting $\delta = 1$ and basing the regression on $E_I$, we find $\varphi_I = 1.58$ and $\Delta G_s^0 = 2.00$ eV. Using instead $E_K$ leads to $\varphi_K = 1.39$, $\Delta G_s^0 = 1.56$ eV. Individual fits of each formamide solution yield $\varphi_K = 2.62$ and $\Delta G_s^0 = 2.08$ eV for F22, $\varphi_K = 1.46$ and $\Delta G_s^0 = 1.62$ eV for F16, and $\varphi_K = 2.20$ and $\Delta G_s^0 = 1.94$ eV for F14. These wide variations of $\varphi$ and $\Delta G_s^0$ are almost surely associated to the fact that we can detect ions from the meniscus only when their current becomes comparable to the total spray current. Under these conditions, the meniscus field cannot be expected to be given very accurately by either $E_K$ or $E_I$, since the corresponding scaling laws have been obtained outside the ion evaporation regime. Therefore, the rules giving the field in terms of the control variables $K$, $I$ and $Q$ can be trusted only near the threshold fields in Fig. 17.

### D. Ion evaporation and suppression of Coulomb explosions

We have seen in Fig. 8 that the Coulomb fissions present at the two larger flow rates disappear at the smallest flow shown. This suppression of the second step is due to the fact that the drops reach the critical field necessary for evaporating the excess charge faster than it takes to undergo a Coulomb fission. The same phenomenon is illustrated in Figs. 18(a)–18(c) through the stopping potential curves of solutions F02, F07 and F14 taken at 0.02 mTorr. Since electro-

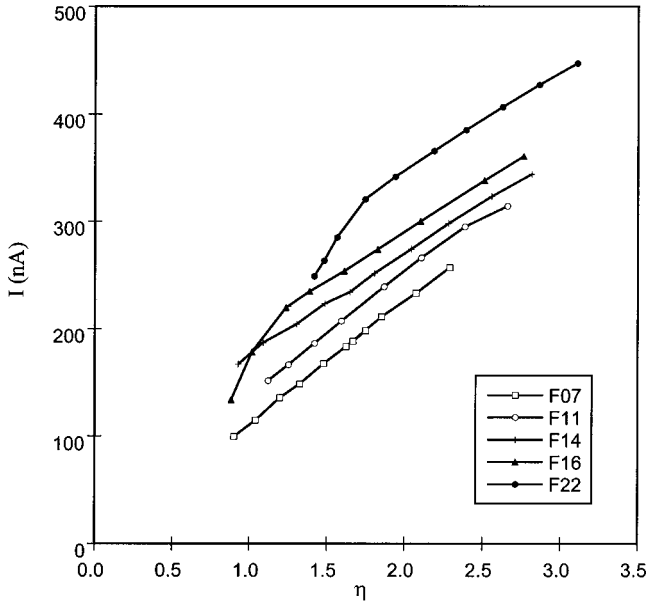


FIG. 16. Current associated with droplets for several formamide solutions.

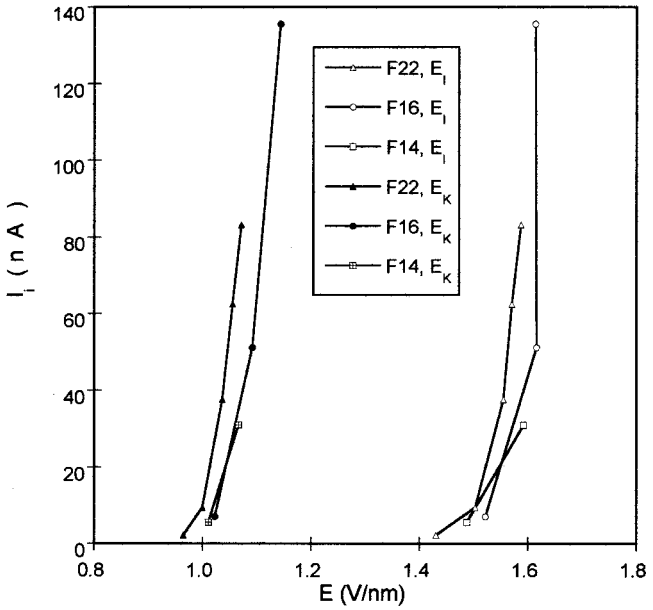


FIG. 17. Ion current evaporated directly from the liquid meniscus versus characteristic electric fields $E_I$ [Eq. (5a)] and $E_K$ [Eq. (5b)] for solutions F14, F16 and F22. The onset is at $E_K \sim 1$ V/nm.

spray drops above the Rayleigh limit are unstable, given pairs $Q-I$ or $Q-K$, the necessary condition for the occurrence of a fission is

$$D_d > 2(36\gamma\epsilon_0)^{1/3}\left(\frac{Q}{I}\right)^{2/5} \sim 2\left(\frac{36\epsilon_0}{F^2(\epsilon)}\right)^{1/3}\left(\frac{Q}{K}\right)^{1/3}. \tag{31}$$

The evaporation of charge imposes a second constraint on the diameter of an exploding drop: The electric field associated to its Rayleigh limit must be smaller than $E^*$, the critical value for the onset of charge evaporation. Otherwise, the short time required for evaporating enough charge to decrease the electric field below $E^*$ will avoid the fission process. Therefore, for a fixed pair $(Q,K)$, droplets undergoing Coulomb explosions must be within the range

$$2\left(\frac{36\epsilon_0}{F^2(\epsilon)}\right)^{1/3}\left(\frac{Q}{K}\right)^{1/3} < D_d < \frac{6E^*\epsilon_0}{g(\epsilon)}\left(\frac{1}{\gamma}\right)^{1/2}\left(\frac{Q}{K}\right)^{1/2}. \tag{32}$$

We see that for small enough values of the ratio $Q/K$, the upper bound is smaller than the lower one. Ions would then evaporate from the drop surface, and no range of radii would exist for which the drops could undergo Coulomb explosions. This is actually what is found in Figs. 18(a)–18(c). Due to the high electrical conductivity of F14 (c), its sprays are produced with low values of $Q/K$ (note that the onset of ion evaporation from the cone-jet itself is detected for the lowest flow rates, Fig. 11), and no Coulomb explosions are observed in the stopping potential curves. The opposite is seen for the sprays of F02 (a). Because the values of $Q/K$ are now higher, the largest drops of the sprays explode along the whole range of stability of this solution. Finally, the stopping potential curves of the solution with an intermediate electrical conductivity, F07 (b), present the most interesting feature: at the lowest flow rate the Coulomb explosions are suppressed or, in other words, at this point the value of $Q/K$ is such that the left and right hand sides in Eq. (32) coincide.

Notice that, for $K \geqslant 1.4$ S/m, the ions which evaporate from the drops do so in the earliest stage of their flight. This is evident from the steepness of the stopping potential curves, which show that ions and drops originate at the same voltage, which must be the potential at the jet tip. Liquid evaporation from the drops is therefore negligible in these experiments, as expected from their short times of flight.

The disappearance of Coulomb explosions at the minimum flow rate of F07, Fig. 18(b), can be used to estimate $\Delta G_s^0$ independently. At this precise point every drop which is initially charged slightly above the Rayleigh limit, has an electric field high enough to field evaporate this charge before the occurrence of the fission. The rate is large enough for the assumption $\Psi \gg 1$ to be adequate in Eq. (23), leading to

$$At = 2\Psi_0^{-1}\exp[-\Psi_0]. \tag{33}$$

The continuous disappearance of Coulomb explosions as the flow rate is decreased clearly indicates that at the minimum flow rate, all the droplets are charged, at most, at the Rayleigh limit. Therefore, $\Psi_0$ must be computed at the Rayleigh limit for a drop with volumetric charge equal to $I_m/Q_m$, where the subscript $m$ stands for the minimum values.

$$\Psi = \frac{1}{kT}\left(\frac{e^3E_m}{4\pi\epsilon_0}\right)^{1/2}, \tag{34}$$

$$E_m = \left(\frac{I_m}{Q_m}\frac{4\gamma}{3\epsilon_0^2}\right)^{1/3}. \tag{35}$$

Let us now estimate the time in Eq. (33) available for ion evaporation. $t$ must be comparable to the characteristic time $t_R$ required for a Coulomb explosion. Two characteristic times might appear depending on whether inertial, $t_{R\rho}$, or viscous forces, $t_{R\mu}$, control the fission process

$$t_{R\rho} \sim \left(\frac{R^3\rho}{\gamma}\right)^{1/2}, \tag{36}$$

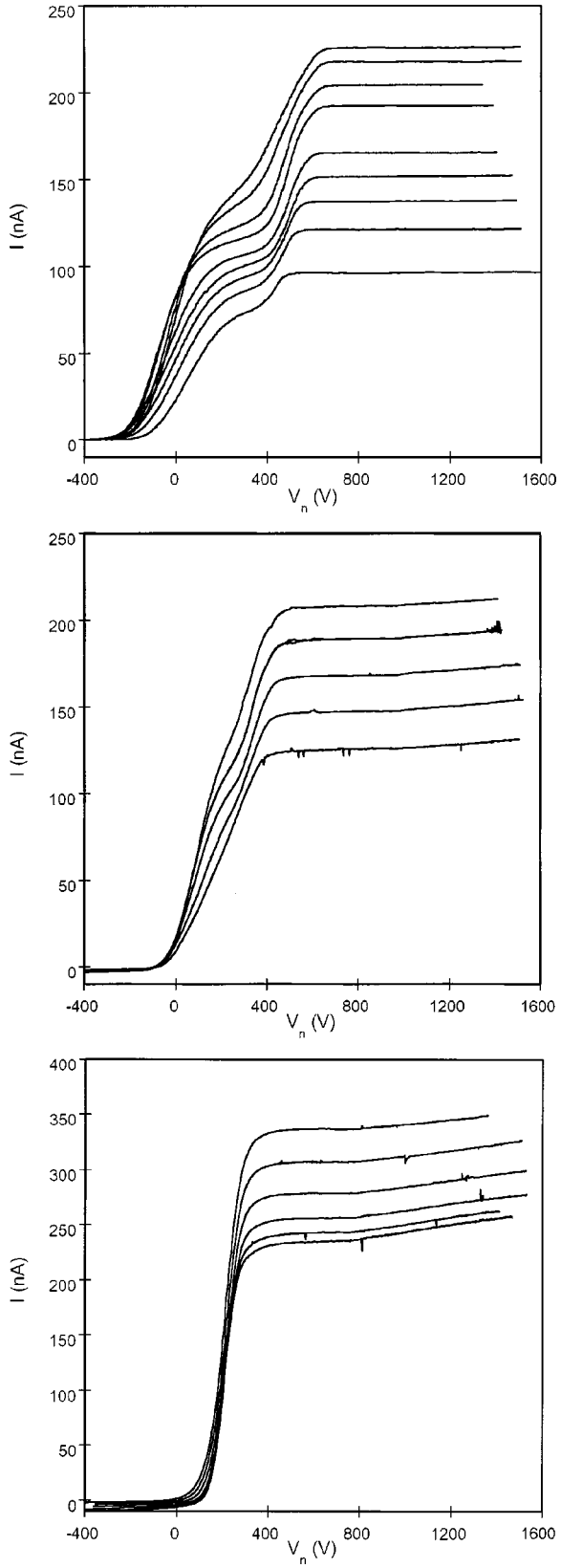


FIG. 18. Disappearance of Coulomb explosions (second step) at decreasing flow rate and increasing electrical conductivity for solutions F02 (a), F07 (b) and F14 (c).

$$t_{R\mu} \sim \frac{R\mu}{\gamma}. \tag{37}$$

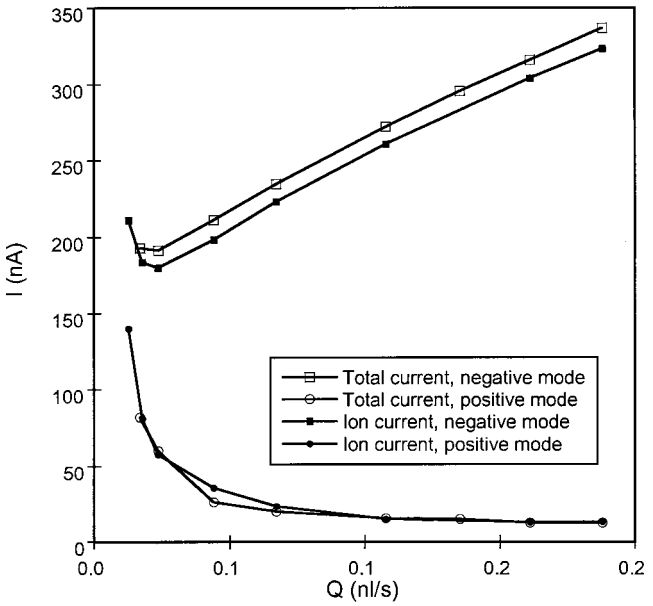


FIG. 19. Magnitude of spray and ion current versus flow rate for solution F14 in positive and negative modes. No significant effect of polarity is observed.

A third possible estimate for $t$ is computed from the equation of motion of a drop which evaporates its excess charge while traveling some tens of volts, $\Delta V$, in the potential field (we have pointed out above that the evaporation of charge from drops in flight must occur very close to the point of formation of the drop). Taylor's solution, $V \sim (\gamma x/\epsilon_0)^{1/2}$, is used for the potential field to render $t_T$

$$t_T \sim 0.86 \frac{\epsilon_0}{\gamma} \left( \frac{m}{2q} \right)^{1/2} \Delta V^{3/2}. \tag{38}$$

$m$ and $q$ stand for the mass and charge of the drop. The curve for the minimum flow rate in Fig. 18(b) has been associated with the values 124 nA and 0.064 nl/s for $I_m$ and $Q_m$, respectively. These numbers yield $\Psi = 51.9$ and $R = 17.0$ nm. The electric field has a value of 1.24 V/nm. If this threshold field for ion evaporation from the drops is taken to coincide with that for ion evaporation from the meniscus ($E_K \sim 1$ V/nm), this would fix the geometrical constant $\varphi$ as $\varphi_K = 1.24$. Interestingly, this value is only slightly larger than the lower bound 1.19 obtained in Eq. (11). The estimates for the three ion evaporation times are $t_{R\rho} \sim 0.30$ ns, $t_{R\mu} \sim 1.1$ ns and $t_T \sim 2.2$ ns (we have assumed a potential drop of 100 V to compute $t_T$). The similarity between the three estimates is noteworthy. Using the mean value $t_{R\mu}$ in (33) yields $\Delta G_s^0 = 1.65$ eV.

### E. Evaporation of $I^-$ anions

We have investigated the evaporation of $I^-$ ions in negative mode from the same formamide solutions discussed ear lier under positive mode, using the same experimental set up except for the inversion of polarities for all the electrodes within the electrospray chamber. Figure 19 plots the absolute

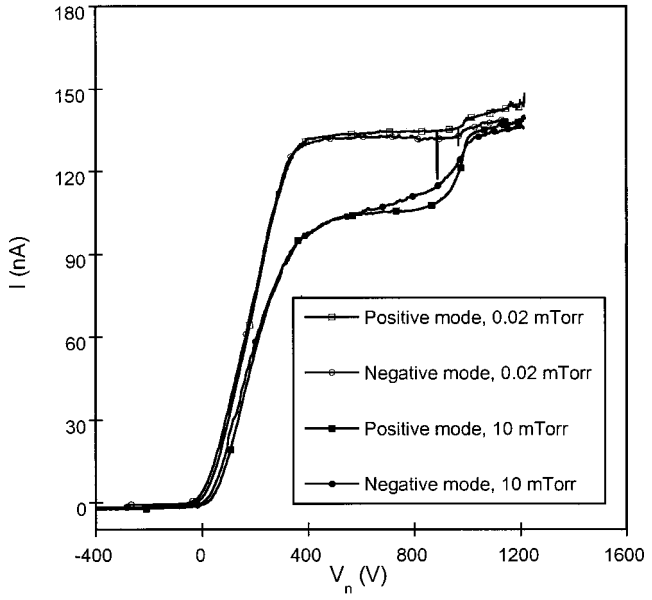


FIG. 20. Stopping potential curves for solution F07 at 0.02 mTorr and 10 mTorr. The electrosprays are run in positive and negative mode, respectively. Lighter $Na^+$ is more easily stopped than $I^-$.

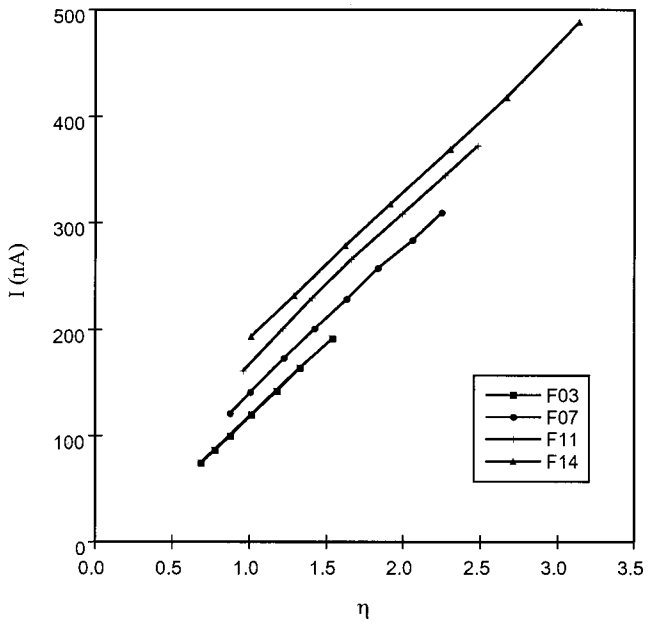


FIG. 21. Spray current versus dimensionless flow rate for several solutions under atmospheric conditions. The onset of electric gas discharges makes impossible the study of the ion evaporation regime of the cone-jet.

value of the total and ionic currents versus liquid flow rate for solution F14, run at positive and negative modes. No significant difference is noticeable between the characteristic values of the electric field required to evaporate these two ions. This is congruent with the known fact that the Gibbs free energy of solvation of alkali and halogen ions have similar values.[35] This is to be expected for the case of small ions dissolved in liquids of high dielectric constant. In this case molecules of the solvent tend to surround the ion, forming a shell which minimizes the effect of the particular ionic core. But the $I^-$ and $Na^+$ ions have different physical properties also, which reveal themselves in changes of the stopping potential curves. Figure 20 plots four curves obtained with solution F07 at fixed liquid flow rate, in positive as well as negative mode. The familiar change in background pressure is used to resolve the ionic and drop fractions of the current transported by the spray. Although both types of curves are nearly identical in the range of stopping potentials where the drops are collected, some differences appear in the abscissa location between 500 V and 1000 V. These differences are most evident for the data measured at 10 mTorr. $Na^+$ ions (positive mode) are more easily stopped than $I^-$ ions (negative mode), reflecting the considerably large range of the heavier ion. This behavior was observed equally in experiments with F14. An interesting corollary is that these ions must have been desolvated by collisions with the background, since both of them evaporated originally as solvated clusters, with essentially the same mass and cross section. This ion source is hence able to deliver substantial currents of bare halogen ions.

### F. Ion evaporation at atmospheric conditions

It is reasonable to expect that the ion evaporation regime will also occur at atmospheric pressure. We have electrosprayed the same formamide solutions in different background gases (dry air, $CO_2$ and ambient air) at one bar, in order to test this possibility. We observed that, for the most conducting solutions and close to the minimum flow rate, a localized electrical discharge developed in the apex of the cone-jet. For a solution of given electrical conductivity, the exact flow rate at which the discharge was produced was found to depend on the nature of the surrounding gas, and on the voltage difference between the spraying needle and the electrode facing it, in such a way that reproducible results were difficult to obtain. We relate the appearance of discharges, attained well below the breakdown voltage of the background gas, to the evaporation of a substantial ionic current from the jet surface. These ions, produced under electric fields of 1 V/nm, gain a kinetic energy of several tens of eV before their first molecular collision (the mean free path of ambient air at standard conditions is 66 nm), which is apparently enough to start and sustain a localized discharge. Figure 21 plots the dimensionless current versus the dimensionless flow rate for several formamide solutions when the cone-jet is surrounded by dry ambient air at one bar and the needle faces the collector directly. One sees a vertical displacement of the curves for increasing conductivities, as already observed in the vacuum experiments. Although the points of onset of discharges have not been indicated because of their poor reproducibility, we observed that they occur at flow rates lower than those at which ions evaporate from the cone-jet itself under vacuum conditions. Thus, background gas molecules tend to increase the characteristic electric field required for the onset of ion evaporation. This would explain part of the differences between the values of $\Delta G_s^0$ measured in this work and those reported by Tang and Kebarle.[35] Part of the difference must be due also to the different solvents used (formamide and water).

## V. CONCLUSIONS

A regime where ion evaporation occurs at substantial rates from Taylor cones in vacuum has been identified for formamide seeded with NaI at concentrations in the range of 1 M. Ion currents have been separated from those associated with nanometer drops by a combination of stopping potential techniques and preferential deceleration of the ions by a background gas. Three ionization regions are observed as the characteristic $K/Q$ ratio increases. A small initial ion current is attributed to the existence of a few highly curved areas, associated probably with the region of jet break-up and/or to small satellite drops. At higher $K/Q$ values ionization proceeds mostly from the main drops, and at still higher $K/Q$ it is dominated by ion evaporation from the meniscus itself. Only in this last stage does the total spray current increase above its usual value. This leads to a minimum in the $I(Q)$ relation at a characteristic flow rate $Q=Q^*$, with a rapid growth of the total and ionic currents for $Q<Q^*$. These three types of ionization regimes follow a different behavior, and may be separated from each other. The problem of measuring the rate of ionization has therefore been solved satisfactorily.

The problem of controlling the value of the electric field $E$ on the liquid surface leading to the measured ion currents has been approached via available scaling laws for the geometry and charge density of the Taylor cone-jet and the drops. The ratio between $E$ and the characteristic fields $E_K$ and $E_I$ [given in Eqs. (5a), (5b) in terms of measurable physical quantities] is a number $\varphi$ of order one whose precise value is unknown *a priori*. This ambiguity seems to be small for the case of drops, for which $\varphi$ has been provisionally taken to be unity, as if ion emitting drops were spherical through most of the ion evaporation stage. The data for ion evaporation from drops are consistent with this hypothesis, perhaps with an error in $\varphi$ of up to 20%. The activation energy for ion evaporation in the small-field and small-curvature limit is found consistently by several independent techniques based on ion evaporation from the drops to be $1.7\pm0.1$ eV, though the error bar must be taken as provisional. This is considerably smaller than the accepted value 2.2–2.4 eV for the evaporation of $Na^+$ from water in the presence of its vapor.

The ion evaporation current from the meniscus sets in at a critical $E_K$ near 1 V/nm. According to the lower bound Eq. (11), the associated meniscus field exceeds 1.2 V/nm. This is closely consistent with the value 1.24 V/nm measured independently for this same system from the critical condition at which Coulomb explosions are suppressed. Unfortunately, except near this threshold, ion currents from the meniscus are probably too large for the scaling laws for the field to hold, precluding a reliable independent inference of $\varphi$ or $\Delta G_s^0$.

In spite of our inexact knowledge of the value of $E$, all of the measurements made support strongly the ion evaporation model of Iribarne and Thomson, with an activation barrier for ion evaporation equal to $(1.7\pm0.1)\,\mathrm{eV} - (e^3E/4\pi\epsilon_0)^{1/2}$.

## ACKNOWLEDGMENTS

We are in debt with Dr. Iñigo Aguirre-de-Carcer and Dr. Ignacio Loscertales for their initial contributions to the planning of this study. Financial support from the National Science Foundation (Grant No. CTS-9319151) and Yale's Engineering Council is gratefully acknowledged.

[1] J. B. Fenn, M. Mann, C. K. Meng, S. K. Wong, and C. Whitehouse, Science **246**, 64 (1989).
[2] G. J. Van Berkel, J. M. E. Quirke, R. A. Tigani, A. S. Dilley, and T. R. Covey, Anal. Chem. **70**, 1544 (1998).
[3] We are interested mainly in the case of organic liquids, where a wide control of the electrical conductivity $K$ is available. Related literature on *electrospray mass spectrometry* exceeds 1000 articles/year. Although liquid metals will be mentioned a few times, the term ''liquid'' is used to mean water or organic solvents, to the exclusion of ionic liquids, molten salts or liquid metals.
[4] E. W. Muller, Phys. Rev. **102**, 618 (1956).
[5] J. V. Iribarne and B. A. Thomson, J. Chem. Phys. **64**, 2287 (1976).
[6] V. Katta, A. L. Rockwood, and M. L. Vestal, Int. J. Mass Spectrom. Ion Processes **103**, 129 (1991).
[7] I. G. Loscertales, ''Ion emission from charged liquid surfaces,'' Ph. D. thesis, Yale University (1995); I. G. Loscertales and J. Fernández de la Mora, J. Chem. Phys. **103**, 5041 (1995).
[8] Lord Rayleigh, Philos. Mag. **14**, 184 (1882).
[9] Lord Rayleigh, *The Theory of Sound* (Dover, New York, 1945), Sec. 364, p. 374.
[10] B. A. Thomson and J. V. Iribarne, J. Chem. Phys. **71**, 4451 (1979).
[11] B. A. Thomson, J. V. Iribarne, and P. J. Dziedzic, Anal. Chem. **54**, 2219 (1982).
[12] P. D. Prewett and G. L. R. Mair, *Focused Ion Beams from Liquid Metal Ion Sources* (Wiley, New York, 1991); L. W. Swanson, Nucl. Instrum. Methods Phys. Res. **218**, 347 (1983); R. G. Forbes, Vacuum **48**, 85 (1997).
[13] J. Perel, J. F. Mahoney, R. D. Moore, and A. Y. Yahiku, AIAA J. **7**, 507 (1969).
[14] B. P. Stimpson, D. S. Simons, and C. A. Evans, J. Phys. Chem. **82**, 660 (1978).
[15] K. D. Cook, Mass Spectrom. Rev. **5**, 467 (1986). This highly stressed multi-jet regime is poorly understood, making glycerol solutions non ideal for quantitative investigations of the ionization kinetics.
[16] M. Gamero-Castaño, I. Aguirre de Carcer, L. de Juan, and J. Fernández de la Mora, J. Appl. Phys. **83**, 2428 (1998).
[17] G. I. Taylor, Proc. R. Soc. London, Ser. A **280**, 383 (1964).
[18] J. Fernández de la Mora and I. G. Loscertales, J. Fluid Mech. **260**, 155 (1994).
[19] D. R. Chen and D. Pui, Aerosol. Sci. Technol. **27**, 367 (1997).
[20] A. M. Gañán-Calvo, J. Dávila, and A. Barrero, J. Aerosol Sci. **28**, 249 (1997).
[21] L. Cherney, J. Fluid Mech. **378**, 167 (1999); J. Aerosol Sci. **30**, 851–862 (1999).
[22] J. Rosell-Llompart and J. Fernández de la Mora, J. Aerosol Sci. **25**, 1093 (1994).
[23] R. L. Hines, J. Appl. Phys. **37**, 2730 (1966).
[24] A. M. Gañán-Calvo, Phys. Rev. Lett. **79**, 217 (1997).
[25] K. Tang and A. Gomez, Phys. Fluids **6**, 2317 (1994).
[26] L. de Juan and J. Fernández de la Mora, J. Colloid Interface Sci. **186**, 280 (1997).
[27] A. M. Gañán-Calvo, J. C. Lasheras, J. Dávila, and A. Barrero, J. Aerosol Sci. **25**, 1121 (1994).
[28] M. Gamero-Castaño, ''The transfer of ions and charge nanoparticles from solution to the gas phase in electrosprays,'' Ph. D. thesis, Yale University (1999).
[29] M. N. Huberman, J. Appl. Phys. **41**, 578 (1970).
[30] J. A. Riddick, W. B. Bunger, and T. K. Sakano, *Organic Solvents. Physical Properties and Methods of Purification*, 4th ed. (Wiley, New York, 1986).
[31] $\Psi$ must be large in the ion evaporation regime, since $\Delta G_s^0/kT$ is typically

larger than 50, and the rate would otherwise be astronomically small.
[32] This observation is congruent with earlier findings in so-called EHD ionization (Ref. 15), where glycerol solutions with $K$ as small as 0.02 S/m produce measurable ionic currents.
[33] J. Rosell-Llompart, ''Size characterization in electrosprays of submicron droplets,'' Ph. D. thesis, Yale University (1994).
[34] L. de Juan, ''Characterization and generation of charged aerosols by tandem spectrometry and electrospray source,'' Ph. D. thesis, Yale University (1997).
[35] L. Tang and P. Kebarle, Anal. Chem. **65**, 3654 (1993).
[36] M. Gamero-Castaño and J. Fernández de la Mora, Anal. Chim. Acta **406**, 67 (2000).